# Light-driven ultrafast polarization manipulation in a relaxor ferroelectric

Suji Park<sup>1,2</sup>•, Bo Wang<sup>3</sup>•, Tiannan Yang<sup>3</sup>•, Jieun Kim, Sahar Saremi<sup>4,5</sup>, Wenbo Zhao<sup>4</sup>, Burak Guzelturk<sup>1</sup>, Aditya Sood<sup>1</sup>, Clara Nyby<sup>1</sup>, Marc Zajac<sup>1</sup>, Xiaozhe Shen<sup>2</sup>, Michael Kozina<sup>2</sup>, Alexander H. Reid<sup>2</sup>, Stephen Weathersby<sup>2</sup>, Xijie Wang<sup>2</sup>, Lane W. Martin<sup>4,5</sup>, Long-Qing Chen<sup>3</sup>, Aaron M. Lindenberg<sup>1,6,7,\*</sup>

- <sup>1</sup> Stanford Institute for Materials and Energy Sciences, SLAC National Accelerator Laboratory, Menlo Park, CA, 94025, USA.
- <sup>2</sup> SLAC National Accelerator Laboratory, Menlo Park, CA, 94025, USA.
- <sup>3</sup> Department of Materials Science and Engineering, Penn State University, University Park, PA, 16802, USA.
- <sup>4</sup> Department of Materials Science and Engineering, UC Berkeley, Berkeley, CA, 94720, USA.
- <sup>5</sup> Materials Sciences Division, Lawrence Berkeley National Laboratory, Berkeley, CA, 94720, USA.
- <sup>6</sup> Department of Materials Science and Engineering, Stanford University, Stanford, CA, 94305, USA.
- <sup>7</sup> PULSE Institute, SLAC National Accelerator Laboratory, Menlo Park, CA, 94025, USA.

## **Abstract:**

Relaxor ferroelectrics have been intensively studied for decades based on their unique electromechanical responses which arise from local structural heterogeneity involving polar nanoregions or domains. Here, we report first studies of the ultrafast dynamics and reconfigurability of the polarization in freestanding films of the prototypical relaxor 0.68PbMg<sub>1/3</sub>Nb<sub>2/3</sub>O<sub>3</sub>-0.32PbTiO<sub>3</sub> (PMN-0.32PT) by probing its atomic-scale response via femtosecond-resolution, electron-scattering approaches. By combining these structural measurements with dynamic phase-field simulations, we show that femtosecond light pulses drive a change in both the magnitude and direction of the polarization vector within polar nanodomains on few-picosecond time-scales. This study defines new opportunities for dynamic reconfigurable control of the polarization in nanoscale relaxor ferroelectrics.

Keywords: ferroelectrics, structural dynamics, ultrafast, electron diffraction

<sup>•</sup>These authors contributed equally

<sup>\*</sup>Corresponding author: Aaron M. Lindenberg (aaronl@stanford.edu)

Relaxor ferroelectrics are a subgroup of ferroelectrics exhibiting characteristics such as dynamic polar nanoregions (PNRs) or polar nanodomains (PNDs), dynamic disorder and heterogeneity at the nanoscale, and unusually high dielectric and piezoelectric constants, enabling unique functionalities [1-5]. For example, (1-x)PbMg<sub>1/3</sub>Nb<sub>2/3</sub>O<sub>3</sub>-xPbTiO<sub>3</sub> (PMN-xPT) and (1-x)PbZn<sub>1/3</sub>Nb<sub>2/3</sub>O<sub>3</sub>-xPbTiO<sub>3</sub> (PZN-xPT) show ultrahigh electromechanical [6] and nonlinear [7] responses. The highest performance is attained for compositions near the morphotropic phase boundary (MPB) [8], where for PMN-0.32PT the crystal structure lies between a rhombohedral and tetragonal phase with the actual structure still the subject of debate [9, 10]. Recent studies reported the existence of intermediate monoclinic phases as it transforms from the rhombohedral to tetragonal phases, associated with a polarization rotation [11-14]. Additional studies have reported polarization rotation induced by temperature, electric fields, and stress [15-17], thought to underlie the anomalous electromechanical response of the relaxors and other ferroelectrics and the mechanisms for polarization switching [16, 18, 19]. The intrinsic time-scales for these processes to occur have not been measured, of central importance to the application of these materials within switchable devices. In particular, the intrinsic dynamic and nanoscale nature of the PNDs and associated low-energy barriers [9] indicate the potential for new opportunities for modulating the ferroelectric polarization on ultrafast time-scales [20-27].

Here, the light-induced ultrafast structural changes of an unpoled [001]-oriented PMN-0.32PT freestanding film are probed by femtosecond MeV electron scattering. By measuring the structure factor of many Bragg peaks using an ultrafast crystallographic approach, we show that above-gap photoexcitation drives a reconfiguration of the polarization within PNDs on few picosecond time-scales. We propose a simple statistical model showing how the polarization distribution impacts the structure factor of a range of probed Bragg reflections. Our results indicate a significant light-induced reduction in the in-plane polarization within each PND, appearing in the ensemble averaged diffraction measurement as a reduction in the in-plane mean square displacements. By combining these experimental results with phase-field simulations we show that these atomic-scale changes can be understood in terms of an ultrafast modulation of the polarization magnitude coupled to a dynamic rotation of the polarization occurring on picosecond time-scales.

50nm thick PMN-0.32PT/ 10nm La<sub>0.7</sub>Sr<sub>0.3</sub>MnO<sub>3</sub> (LSMO)/ SrTiO<sub>3</sub> (001) heterostructures were grown by pulsed-laser deposition (see Figure 1 and Supporting Information). Following growth, the PMN-0.32PT films were released from the substrate by selective etching of the sacrificial LSMO layer. The unclamped thin films were then removed from the substrate by slowly dipping the substrate in deionized water leaving the freestanding films floating on the water surface. The released films were then moved to a secondary substrate (PDMS or "holey" grid) (Fig. 1c) [28]. We conducted femtosecond time-resolved electron diffraction measurements using the SLAC MeV-UED setup (Fig. 1b) [29]. Above-band-gap (4.5 eV) femtosecond optical pulses were used as a trigger on a PMN-0.32PT freestanding film ( $E_g \approx 3.5 \text{ eV}$ ) [30], probing the diffraction pattern using 3 MeV, 20 fC electron bunches at 180 Hz. By changing the delay time of the laser relative to the electron beam, we collected femtosecond-resolved diffraction patterns to capture the reversible structural response averaged over many shots and for a range of fluences from 2.6 mJ/cm<sup>2</sup> to 7.8 mJ/cm<sup>2</sup>.

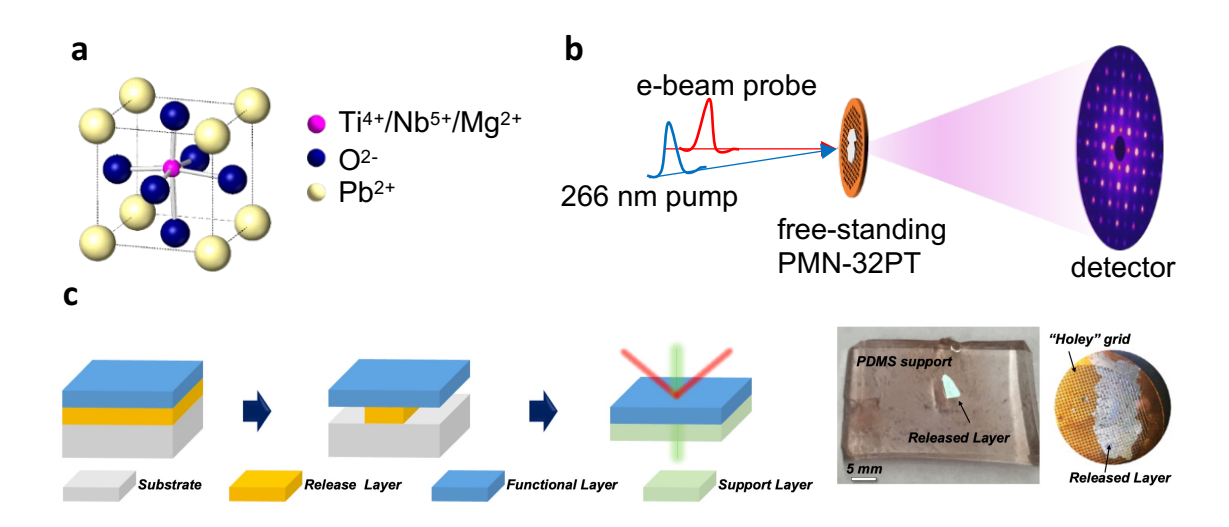


**Figure 1. The structure of PMN-***x***PT and experimental setup. a.** Crystal structure of PMN-*x***PT. b.** 266nm pump – UED probe experimental setup. **c.** Freestanding relaxor membrane sample synthesis.

Figure 2a shows the measured static electron diffraction pattern along the [001] zone axis at 28 K corresponding to (hk0) Bragg peaks where h,k, and l(=0) are the Miller indices of the reflection. From the images taken at each time delay, we extracted the intensity of the Bragg

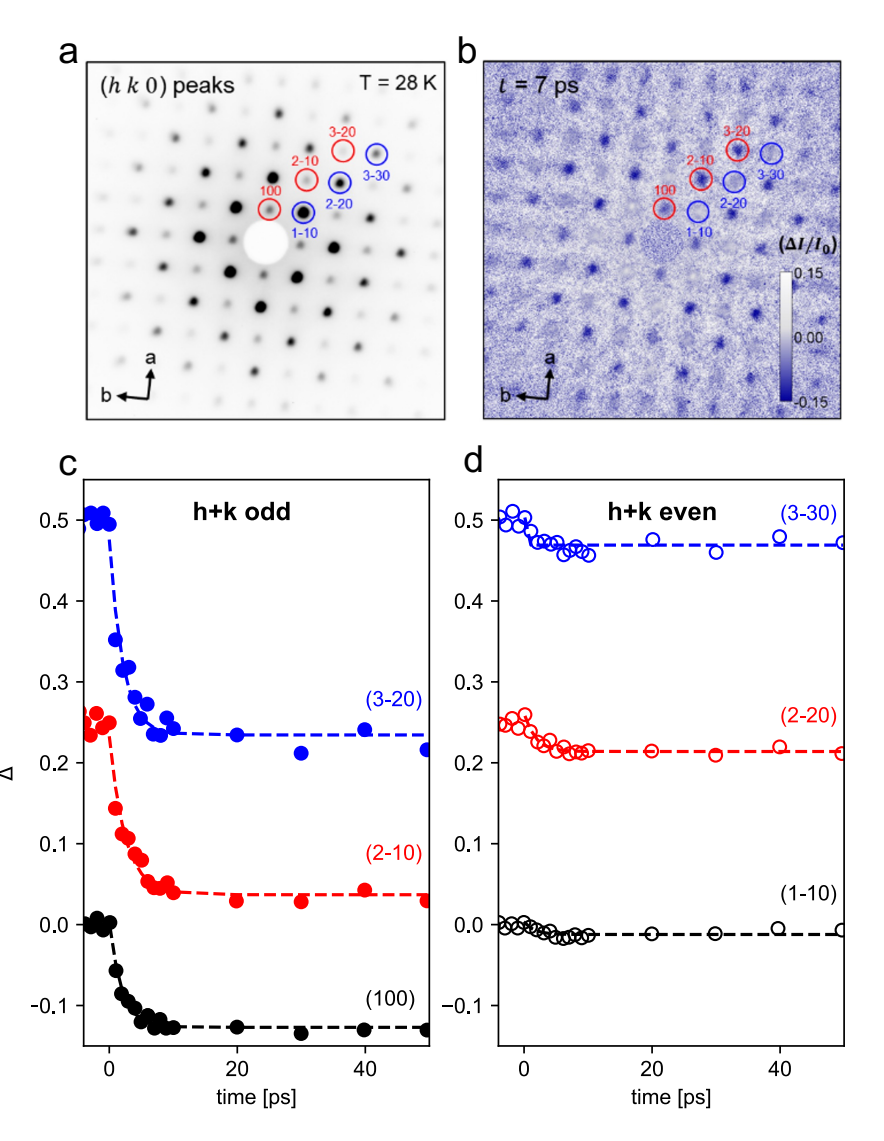


Figure 2. Transient diffraction pattern and time-resolved response of Bragg peaks. a. raw image showing UED diffraction data at 28K probing along [001] zone axis. b. Fractional change  $\Delta I/I=(I-I_0)/I_0$  at t=7 ps. The red and blue circles define h+k= odd and even peaks respectively. c and d. The intensity changes of representative odd (c) and even (d) peaks. Dashed lines are exponential fits with time constant  $\sim 2$  ps.

peaks,  $I_{hkl}$ , and tracked the fractional intensity changes of each peak ( $\Delta I/I_0$ ) where  $I_0$  is the static intensity (corresponding to delay times t < 0). Figure 2b displays a representative image showing the differential intensity change at t = 7 ps. We note a strong anisotropy in the differential intensity changes for the measured Bragg reflections, with h + k = 0 odd peaks (red circles) showing significant intensity drop as opposed to h + k = 0 even peaks (blue circles). The time-dependent intensity change of representative peaks with h + k odd are shown in Figure 2c and h + k even in Figure 2d. The graphs similarly show that the intensity of odd parity peaks drops dramatically ( $\frac{\Delta I}{I_0} \approx 10\%$ ) on few picosecond time-scales (exponential fitted time constant

~2.1 ps) as opposed to even peaks showing much smaller changes. With increasing momentum transfer the effect becomes larger in both even and odd cases.

To understand the measured dynamic intensity changes of the Bragg peaks, we introduce a statistical structure factor model to capture how off-centering of the central B-site cations influence the scattered intensity of a given Bragg peak. We note that this model does not differentiate between whether the A- or B-site cations move — only their relative position determines the interference effects which define the intensity of each peak — and it ignores, to first order, any dynamic response from the oxygen octahedra. Although the nature of relaxors near the MPB is a mixture of various domains and crystal structures, *i.e.*, rhombohedral (R), monoclinic (M), and tetragonal (T) phases [11-13], here we assume a standard cubic perovskite structure as an averaged unit cell with an off-centered B-site cation displaced by small parameters  $\delta_x$ ,  $\delta_y$ , and  $\delta_z$  along the x, y, and z directions, respectively, with the z direction pointing along [001] (normal to the film). The intensity of the diffracted beam is determined from the structure factor,  $F_{hkl}$ , the Fourier transform of the unit cell, which can be written as:

$$F_{hkl} = \sum_{n} f_n e^{2\pi i (hx_n + ky_n + lz_n)} \quad (1)$$

Here,  $f_n$  is the scattering factor of the  $n^{\text{th}}$  atom. With a *B*-site cation at position  $(\frac{1}{2} + \delta_x, \frac{1}{2} + \delta_y, \frac{1}{2} + \delta_z)$  and for the [001] zone axis with l = 0, one obtains:

$$F_{hk0} = \begin{cases} f_{Pb} - f_0 - f_B e^{2\pi i (h\delta_x + k\delta_y)} & h + k \text{ odd} \\ f_{Pb} + 3f_0 + f_B e^{2\pi i (h\delta_x + k\delta_y)} & h, k \text{ both even} \\ f_{Pb} - f_0 + f_B e^{2\pi i (h\delta_x + k\delta_y)} & h, k \text{ both odd} \end{cases}$$
(2),

where  $f_{Pb}$ ,  $f_O$ , and  $f_B$  are the scattering factors for the lead, oxygen, and B-site atoms, respectively, and are assumed to be time independent. One may understand, from this expression, the origin of the bright and dark peaks shown in Figure 2A, with the weakest peaks associated with those with h+k odd where the scattering from the lead and B-site cations destructively interfere. To calculate the measured ensemble-averaged intensity we note that the approximate diameter of a PND ( $\approx 10$  nm) [3] is larger than the transverse coherence of the electron beam ( $\approx 1$  nm). Thus we compute the scattered intensity by first calculating the modulus squared of the unit cell structure factor  $|F_{hk}|^2$  and then ensemble averaging over all unit cells (corresponding to a no-interference condition of the scattered fields between different unit cells within a PND) [21, 31]. In the limit where the in-plane displacements  $\delta_x$  and  $\delta_y$  are small compared to the lattice spacing and isotropic, statistically averaging to zero such that there is no net polarization of the

sample, we define the root-mean-square (RMS) displacements  $\sqrt{\langle \delta_x^2 \rangle} = \sqrt{\langle \delta_y^2 \rangle} = \sigma_{xy}$  as a measure of the local unit cell dipole and assume negligible correlations between orthogonal displacements, e.g.,  $\langle \delta_x \delta_y \rangle = 0$ . The measured intensity  $I_{hkl}$  can then be written as

$$I_{hk0} \propto \begin{cases} (A_{hk} - f_B)^2 + 4Af_B \,\pi^2 (h^2 + k^2) \sigma_{xy}^2 & h + k \text{ odd} \\ (A_{hk} + f_B)^2 - 4Af_B \,\pi^2 (h^2 + k^2) \sigma_{xy}^2 & h + k \text{ even} \end{cases}$$
(3),

where  $A_{hk}$  includes the contributions from the lead and oxygen ions and is given by  $A_{hk} = f_{Pb} + 3f_0$  if both h and k are even, otherwise  $A_{hk} = f_{Pb} - f_0$ . As noted above, this result is consistent with the observed static diffraction pattern dependence on the parity of h + k. It is also possible to understand from this result the origin of the anisotropy in the time-dependent response. Under the approximation that photoexcitation modulates the spread of in-plane RMS displacements by an amount  $\Delta \sigma_{xy}$ , we can write the normalized change in the intensity of the (hkl) peak as:

$$\frac{\Delta I}{I} \approx \begin{cases} \frac{4A_{hk} f_B \pi^2 (h^2 + k^2) \Delta \sigma_{xy}^2}{(A - f_B)^2} & h + k \text{ odd} \\ \frac{4A_{hk} f_B \pi^2 (h^2 + k^2) \Delta \sigma_{xy}^2}{(A + f_B)^2} & h + k \text{ even} \end{cases}$$
(4).

In a model in which the light-induced modulation corresponds to a reduction in the RMS inplane displacements corresponding to a reduction in the in-plane dipole within each PND, this equation predicts the observed strong dependence on the parity of h + k, with the largest effects for odd parity reflections, and with the intensity decreasing as experimentally observed for a decrease in the RMS spread of B-site cations. Significantly smaller amplitude changes are predicted by this model for the even reflections, as also observed experimentally, however, with opposite sign. One expects additional light-induced disorder in the form of Debye-Waller contributions[32] to all Bragg peaks associated with additional RMS disorder in the unit cell which likely explains the smaller decreases observed for h+k even.

In the following we apply a more detailed fitting procedure to check the validity of the above model and quantify the induced changes in the unit cell. We assume the distribution of *B*-site cations satisfies a Gaussian distribution, *e.g.*,  $\delta_n = N(\mu_n, \sigma_n^2)$  (for n=x,y) for both the static and non-equilibrium structure [33]. First, we attempted to find the distribution of *B*-site cations in the *xy*-plane before and after laser exposure. Using a least-square method, we found the best fit where the combination of the initial and final distribution minimizes the sum of squared

residuals, SSR =  $\Sigma \left( \frac{\Delta I_{\rm exp}}{I_{\rm exp,i}} - \frac{\Delta (I_{hkl})_i}{(I_{hkl})_i} \right)^2$ . We calculated the SSR with all possible combinations of the initial and final distribution in the range of  $0 < \sigma_{xy,i}$  (or  $\sigma_{xy,f}$ ) < 0.15 with a step size of 0.0003. In order to capture the small amplitude and Q-dependent decreases in the even parity peaks we include for all reflections a standard Debye-Waller term as an additional means to modulate the intensity of each peak [34]. We present the SSR with respect to  $\sigma_{xy,i}$  and  $\Delta \sigma_{xy}$  in Figure 3a. The best fit was found at  $\sigma_{xy,i} = 0.0492$  and  $\Delta \sigma_{xy} = -0.0105$ , corresponding to an approximately 20% reduction (~5 pm) in the in-plane RMS displacements. The minimum SSR is achieved when  $\Delta \sigma_{xy} < 0$  (Fig. 3a) regardless of the initial distribution  $\sigma_{xy,i}$ . This result is consistent with the above presented model, indicating the *B*-site cations moved towards the symmetric position within the *xy*-plane. Figure 3b shows that the intensity change of a range six selected Bragg peaks calculated with the best fit values  $\sigma_{xy,i}$  and  $\sigma_{xy,f}$  (blue bars) match well with the experimental data (maroon).

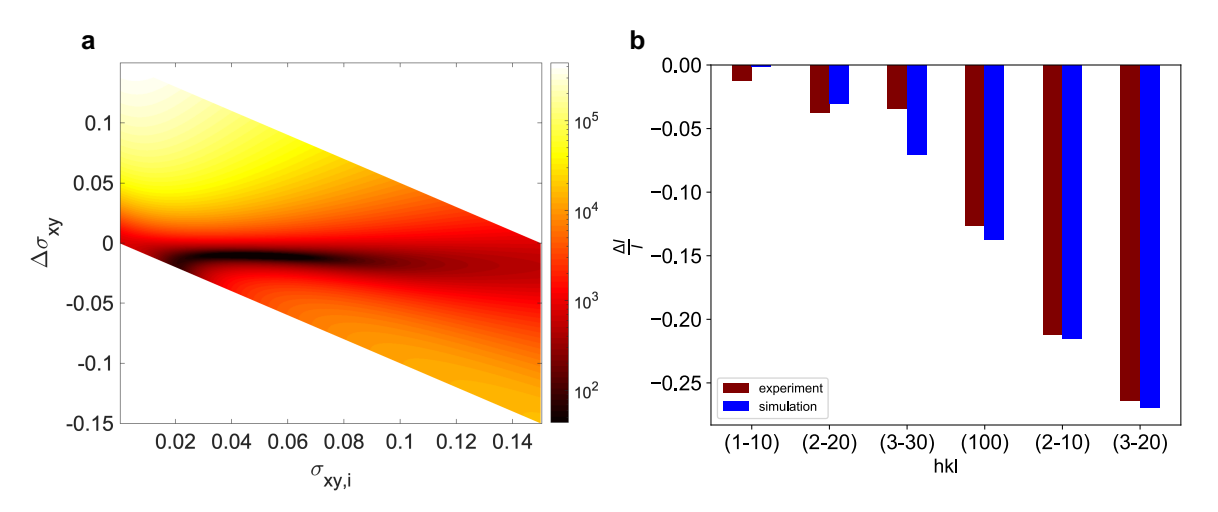
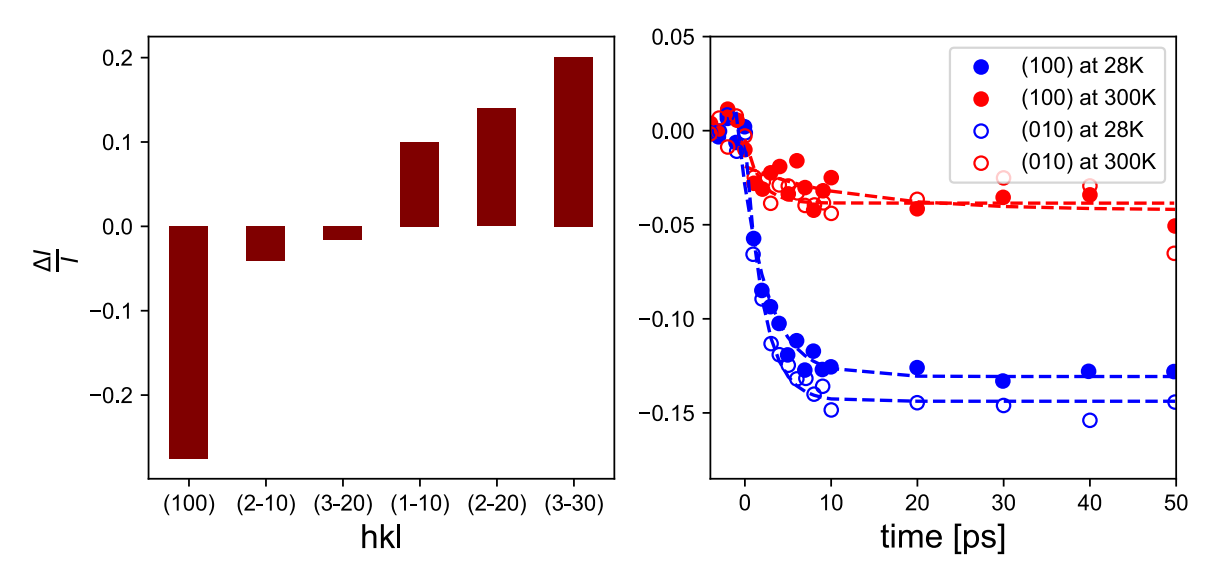


Figure 3. Structure factor model for change in unit cell. a. The sum of squared residuals (SSR) as a function of the change in RMS displacements  $\Delta \sigma_{xy}$  and the initial value  $\sigma_{xy,i}$ . Minimum SSR occurs at  $\Delta \sigma_{xy} = -0.01$  at  $\sigma_{xy,i} = 0.05$ , indicating the RMS displacements of B-site atoms are reduced in the transient state. b. Intensity changes at t=7 ps comparing experiment to structure factor simulation.

In order to understand the mechanism for the light-induced modulation of the unit-cell, we also measured changes in the same PMN-0.32PT sample under a static temperature jump comparable to that estimated to be induced by the absorbed light pulse, approximately 100 K (see Supporting Information) and performed time-resolved measurements at various initial temperatures. Figure 4a shows the observed temperature-induced modulations comparing the Bragg peak intensities at 28K to 150K. This shows effects qualitatively consistent with the structure-factor model presented above, with odd-parity reflections decreasing and even-parity

reflections increasing. Therefore this indicates the important role of a light-induced temperature jump in driving the observed reconfiguration of the structure towards a higher symmetry state. A similar decrease in the polar displacement and standard deviation of the Ti atom as a function of increasing temperature in PMN-25PT has recently been observed by neutron total scattering [35]. To further support the critical role of a temperature jump in the observed transient response, Figure 4b shows the transient response of the (100) reflection comparing room temperature (300 K) to the response at 28 K. This shows a dramatic increase in the magnitude of the distortions at low temperature and is consistent with the significantly smaller heat capacity of typical perovskite oxides at low temperature  $(c_p(30\text{K})/c_p(300\text{K})) \approx$ 1/7 for PZT [36]) leading to more significant photo-induced temperature changes at low temperature, assuming constant absorbed pulse energy. A simple estimation using the known optical properties of PMN-xPT (Supporting Information) gives a temperature jump  $\Delta T = 175$ K for  $T_{\text{init}} = 30$  K and  $\Delta T = 25$  K for  $T_{\text{init}} = 300$  K. Finally we note also that the measured fluence dependent response (Supporting Information Fig. S5) shows a roughly linear response up to the highest fluence measured (7.8 mJ/cm<sup>2</sup>), consistent with this model. Additional electronic effects as have been observed in other studies[22, 37-39] may be contributing separately to these responses but one would expect depolarization-field screening effects, for example, to be less important within the disordered structure of the relaxors and for the freestanding films considered here.



**Figure 4. Temperature-dependent response. (a)** Temperature-jump-induced fractional intensity changes of various peaks  $\frac{\Delta I}{I} = \frac{I_{150K} - I_{28K}}{I_{28K}}$  **(b)** Transient response of PMN-PT comparing room temperature to 28 K.

To further evaluate the above model, we carried out phase-field simulations to characterize the dynamics of the polarization in response to a transient temperature jump, using this to establish a relation between the variation of polarization configurations and the change in diffraction-peak intensities which can be directly compared to the experimental results. The initial polarization configurations is obtained by evolving the system from a random-noise polarization distribution (Fig. 5a). The resultant domain structure is characterized by a mosaic morphology consisting of nano-sized domains with a characteristic length scale of  $\sim$ 10 nm. The broadened peaks in the statistical distribution of in-plane polarization suggests the presence of a local monoclinic distortion of the lattice, resulting in the deviation of the polarization from the nominal  $<111>_{pc}$  direction, as observed experimentally in relaxor crystals and freestanding membranes [40, 41]. In the phase-field simulations transient photoexcitation is modeled as an instantaneous and spatially uniform temperature jump over the entire simulation system, accompanied by a uniform thermal strain due to thermal expansion (for a detailed description see Supporting Information).

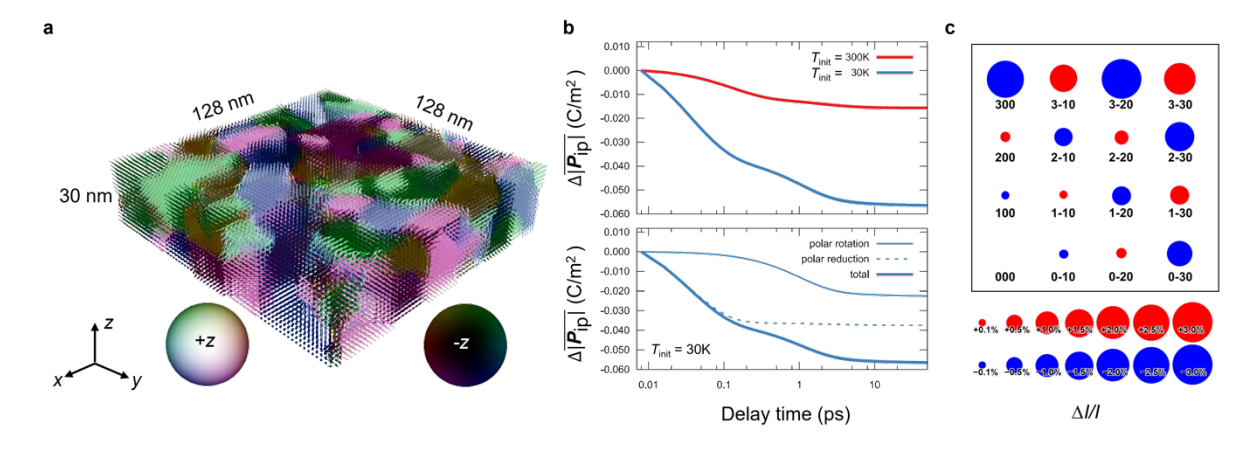


Fig. 5. Phase-field simulations. a) Phase-field simulation of the initial domain morphology and polarization configuration of the PMN-PT freestanding membrane. (a) The simulated initial polarization spatial distribution in 3D for  $T_{\rm init}=30~{\rm K}$ , showing the mosaic domain morphology and the characteristic domain size ~10 nm. The 3D polarization vectors are colored by the direction of  $P_{ip}=(P_x,P_y)$  while the relative brightness corresponds to the magnitude and sign of  $P_z$  ( $P_z>0~{\rm bright}$ ;  $P_z<0~{\rm dark}$ ). b) Phase-field simulation of the temporal evolution of the average change of in-plane polarization  $\Delta |\overline{P_{ip}}|$  (where  $|P_{ip}|=\sqrt{P_x^2+P_y^2}$ ) after the onset of laser pulse at  $t=0~{\rm ps}$ . The upper panel shows  $\Delta |\overline{P_{ip}}|$  for two different initial temperatures,  $T_{\rm init}=30~{\rm K}$  (blue curve with dots) and  $T_{\rm init}=300~{\rm K}$  (red curve with dots). The lower panel shows the contribution to  $\Delta |\overline{P_{ip}}|$  due to polarization rotation (solid), polarization reduction (dashed), and their combination (curve with dots) for  $T_{\rm init}=30~{\rm K}$ . The onset of the laser pulse is modeled as an instantaneous temperature jump with associated thermal expansion strains. (c) The calculated diffraction intensity changes  $\Delta I/I$  for selected peaks around the origin in reciprocal space based on the polarization

configurations obtained by phase-field simulations from t = 0 to t = 50 ps, for  $T_{\text{init}} = 30$  K. The red (blue) color shows an increase (decrease) of the diffraction intensity while the radius denotes the amplitude of the change.

In response to the stimuli, the local ferroelectric polarization in the membrane will change in magnitude and direction to dissipate the injected energy. The variation of the averaged in-plane polarization  $\Delta |P_{ip}|$  (where  $|P_{ip}| = \sqrt{P_x^2 + P_y^2}$  for each spatial point) with respect to the simulation time is plotted in Figure 5b, for two initial temperatures,  $T_{\text{init}} = 30 \text{ K}$  and 300 K in order to compare to the experimental results. The simulation results show that  $|P_{ip}|$  reduces instantly upon the onset of the laser pulse and saturates after ~10 ps consistent with the experimental results. A significantly enhanced reduction is seen for the case with low initial temperature, *i.e.*,  $\frac{\Delta |\overline{P_{lp}}|(T_{init}=30\text{K})}{\Delta |\overline{P_{lp}}|(T_{init}=30\text{K})} = 2.9$ , which reasonably agrees with the intensity modulations in the experiment, *i.e.*,  $\frac{\Delta I/I(T_{init}=30\text{K})}{\Delta I/I(T_{init}=300\text{K})} \approx 3.3$ . Figures S1-S4 in the Supplementary Materials shows further calculations of the spatial distribution of the domains, the temperaturedependence of the statistical distribution of the local polarization, and the relative contributions from a temperature jump compared to an associated elastic strain to the time-dependent polarization response. A closer examination of the temporal evolution reveals two features of polarization relaxation at different regimes before saturation: regime 1 from t = 0 to 0.1 ps and regime 2 from t = 0.1 to 10 ps. From the phase-field simulations, we find that the two regimes correspond to two mechanisms of polarization relaxation, namely, polarization reduction and polarization rotation, both of which contribute to the decrease of  $|P_{ip}|$ , as shown in the lower panel of Figure 5b. The polarization reduction occurs first in response to the laser pulse and dominates in regime 1 and saturates while the polarization rotation proceeds afterwards in regime 2 and saturates at ~10 ps reaching approximately 5 degrees (Fig. S3, Supporting Information). At the final saturated state (t = 50 ps), the polarization reduction corresponds to ~60% of the overall change of  $|P_{ip}|$  while the polarization rotation accounts for ~40%.

To further corroborate the above model, we calculated the diffraction intensities of different Bragg peaks based on the phase-field simulations of the polarization response (additional details in the Supporting Information). The percentage change of Bragg peak intensities upon applying the light pulse for  $T_{\text{init}} = 30 \text{ K}$  is presented in Figure 5c. As seen, the simulated polarization response will cause an intensity decrease (blue circles) at peaks with indices h + k

odd, and a significantly smaller increase (red circles) for h + k even, consistent with experimental observations and the simple analytical model presented above. A list of the calculated Bragg peak intensities before and after light excitation is provided in Supplemental Table S1).

In summary, our time-resolved electron diffraction results show that the polarization state in the relaxor ferroelectric PMN-0.32PT can be significantly and reversibly modulated on picosecond time-scales through above-gap photoexcitation. Using scattering approaches which provide access to the statistical properties of the relaxor polarization state and their dynamics, our measurements, combined with phase-field simulations, show that the polarization within polar nanodomains in relaxor ferroelectrics can be controlled both in magnitude and direction, in particular showing new possibilities for driving ultrafast polarization rotations. Experiments probing tilted samples would provide further information on the out-of-plane polarization dynamics. Additionally, exploration of other stochiometries near the morphotropic phase boundary would usefully inform the correlation between electromechanical responses and the dynamics of the polarization reported here. Finally, future efforts using nanofocused probe beams, diffuse scattering, and/or the use of coherent imaging/speckle techniques in the time domain may enable direct probing of polarization dynamics and associated heterogeneous dynamics within electrically and optically biased operating devices [42], and new possibilities for controlling dynamic disorder and heterogeneity at the nanoscale.

## **ACKNOWLEDGEMENTS**

This work was primarily supported by the U.S. Department of Energy, Office of Science, Office of Basic Energy Sciences, under Award Number DE-SC-0012375. SLAC MeV-UED is supported in part by the DOE BES SUF Division Accelerator & Detector R&D program, the LCLS Facility, and SLAC under Contract Nos. DE-AC02–05-CH11231 and DE-AC02–76SF00515. B.G., A.S., C.N., and M.Z. acknowledge support by the Department of Energy, Office of Science, Office of Basic Energy Sciences under contract DE-AC02-76SF00515. \*, The work at UC Berkeley acknowledges the support of the Army Research Office under grant W911NF-21-1-0118, the National Science Foundation under grant DMR-2102895, and the Collaborative for Hierarchical Agile and Responsive Materials (CHARM) under cooperative agreement W911NF-19-2-0119. B.W. acknowledges support by the National Science

Foundation (NSF) through Grant No. DMR-1744213. T.Y. and L.-Q.C. are supported as part of the Computational Materials Sciences Program funded by the U.S. Department of Energy, Office of Science, Basic Energy Sciences, under Award No. DE-SC0020145.

# **AUTHOR DECLARATIONS**

#### **Conflict of Interest**

The authors have no conflicts of interest to disclose.

#### **DATA AVAILABILITY**

The data that support the findings of this study are available from the corresponding author upon reasonable request.

#### SUPPORTING INFORMATION

Sample synthesis, phase-field simulations, calculation of diffraction intensities from phase-field simulations, fluence-dependent response.

#### **REFERENCES**

- 1. L. E. Cross. "Relaxor ferroelectrics," *Ferroelectrics* **76**, 241-267 (1987).
- 2. A. Fernandez, M. Acharya, H.-G. Lee, J. Schimpf, Y. Jiang, D. Lou, Z. Tian, L. W. Martin. "Thin-film ferroelectrics", *Advanced Materials* 2108841 (2022).
- 3. F. Li, S. Zhang, D. Damjanovic, L.-Q. Chen, T. R. Shrout. "Ferroelectrics: Local Structural Heterogeneity and Electromechanical Responses of Ferroelectrics: Learning from Relaxor Ferroelectrics," *Advanced Functional Materials* **28**, 1870262 (2018).
- 4. F. Li, S. Zhang, T. Yang, Z. Xu, N. Zhang, G. Liu, J. Wang, J. Wang, Z. Cheng, Z.-G. Ye, J. Luo, T. R. Shrout, L.-Q. Chen. "The origin of ultrahigh piezoelectricity in relaxor-ferroelectric solid solution crystals," *Nature Communications* 7, 13807 (2016).
- 5. H. Takenaka, I. Grinberg, S. Liu, A. M. Rappe. "Slush-like polar structures in single-crystal relaxors," *Nature* **546**, 391-395 (2017).
- 6. S.-E. Park, T. R. Shrout, "Ultrahigh strain and piezoelectric behavior in relaxor based ferroelectric single crystals," *Journal of Applied Physics* **82**, 1804-1811 (1997).
- 7. L. M. Riemer, L. Jin, H. Uršič, M. Otonicar, T. Rojac, D. Damjanovic. "Dielectric and electro-mechanic nonlinearities in perovskite oxide ferroelectrics, relaxors, and relaxor ferroelectrics," *Journal of Applied Physics* **129**, 054101 (2021).
- 8. M. J. Krogstad, P. M. Gehring, S. Rosenkranz, R. Osborn, F. Ye, Y. Liu, J. P. C. Ruff, W. Chen, J. M. Wozniak, H. Luo, O. Chmaissem, Z. G. Ye, D. Phelan. "The relation of local order to material properties in relaxor ferroelectrics," *Nature Materials* 17, 718-724 (2018).
- 9. M.E. Manley, D.L. Abernathy, R. Sahul, D.E. Parshall, J.W. Lynn, A.D. Christianson,

- P.J. Stonaha, E.D. Specht, J.D. Budai. "Giant electromechanical coupling of relaxor ferroelectrics controlled by polar nanoregion vibrations," *Science Advances* **2**, e1501814.
- 10. M. Eremenko, V. Krayzman, A. Bosak, H. Y. Playford, K. W. Chapman, J. C. Woicik, B. Ravel, I. Levin. "Local atomic order and hierarchical polar nanoregions in a classical relaxor ferroelectric," *Nature Communications* **10**, 2728 (2019).
- 11. Y. Zhang, D. Xue, H. Wu, X. Ding, T. Lookman, X. Ren. "Adaptive ferroelectric state at morphotropic phase boundary: Coexisting tetragonal and rhombohedral phases," *Acta Materialia* **71**, 176-184 (2014).
- 12. A. K. Singh, D. Pandey. "Evidence for  $M_B$  and  $M_C$  phases in the morphotropic phase boundary region of  $(1-x)[Pb (Mg_{1/3}Nb_{2/3})O_3]-xPbTiO_3$ : A Rietveld study," *Physical Review B* **67**, 064102 (2003).
- 13. R. Wang, H. Xu, B. Yang, Z. Luo, E. Sun, J. Zhao, L. Zheng, Y. Dong, H. Zhou, Y. Ren. "Phase coexistence and domain configuration in Pb(Mg<sub>1/3</sub>Nb<sub>2/3</sub>)O<sub>3</sub>-0.34PbTiO<sub>3</sub> single crystal revealed by synchrotron-based X-ray diffractive three-dimensional reciprocal space mapping and piezoresponse force microscopy," *Applied Physics Letters* **108**, 152905 (2016).
- 14. J. Kim, D. J. Meyers, A. Kumar, A. Fernandez, G. A. P. Velarde, Z. Tian, J.-W. Kim, J. M. LeBeau, P. J. Ryan, L. W. Martin. "Frequency-dependent suppression of field-induced polarization rotation in relaxor ferroelectric thin films, *Matter* **4**, 2367-2377 (2021).
- 15. M. Davis, D. Damjanovic, N. Setter. "Electric-field-, temperature-, and stress-induced phase transitions in relaxor ferroelectric single crystals," *Physical Review B* **73**, 014115 (2006).
- 16. H. Fu, R. E. Cohen. "Polarization rotation mechanism for ultrahigh electromechanical response in single-crystal piezoelectrics," *Nature* **403**, 281-283 (2000).
- 17. F. Li, S. Zhang, T. Yang, Z. Xu, N. Zhang, G. Liu, J. Wang, J. Wang, Z. Cheng, Z.-G. Ye, J. Luo, T. R. Shrout, L.-Q. Chen. "The origin of ultrahigh piezoelectricity in relaxor-ferroelectric solid solution crystals," *Nature Communications* 7, 13807 (2016).
- 18. R. K. Vasudevan, Y. Matsumoto, X. Cheng, A. Imai, S. Maruyama, H. L. Xin, M. B. Okatan, S. Jesse, S. V. Kalinin, V. Nagarajan. "Deterministic arbitrary switching of polarization in a ferroelectric thin film," *Nature Communications* **5**, 4971 (2014).
- 19. S. Prosandeev, B. Xu, L. Bellaiche. "Polarization switching in the PbMg<sub>1/3</sub>Nb<sub>2/3</sub>O<sub>3</sub> relaxor ferroelectric: An atomistic effective Hamiltonian study," *Physical Review B* **98**, 024105 (2018).
- 20. R. Mankowsky, A. von Hoegen, M. Först, A. Cavalleri. "Ultrafast Reversal of the Ferroelectric Polarization," *Physical Review Letters* **118**, 197601 (2017).
- 21. F. Chen, Y. Zhu, S. Liu, Y. Qi, H. Y. Hwang, N. C. Brandt, J. Lu, F. Quirin, H. Enquist, P. Zalden, T. Hu, J. Goodfellow, M. J. Sher, M. C. Hoffmann, D. Zhu, H. Lemke, J. Glownia, M. Chollet, A. R. Damodaran, J. Park, Z. Cai, I. W. Jung, M. J. Highland, D. A. Walko, J. W. Freeland, P. G. Evans, A. Vailionis, J. Larsson, K. A. Nelson, A. M. Rappe, K. Sokolowski-Tinten, L. W. Martin, H. Wen, A. M. Lindenberg. "Ultrafast terahertz-field-driven ionic response in ferroelectric BaTiO<sub>3</sub>," *Physical Review B* **94**, 180104 (2016).
- 22. D. Daranciang, M. J. Highland, H. Wen, S. M. Young, N. C. Brandt, H. Y. Hwang, M. Vattilana, M. Nicoul, F. Quirin, J. Goodfellow, T. Qi, I. Grinberg, D. M. Fritz, M. Cammarata, D. Zhu, H. T. Lemke, D. A. Walko, E. M. Dufresne, Y. Li, J. Larsson, D. A. Reis, K. Sokolowski-Tinten, K. A. Nelson, A. M. Rappe, P. H. Fuoss, G. B. Stephenson, A. M. Lindenberg. "Ultrafast Photovoltaic Response in Ferroelectric Nanolayers," *Physical Review Letters* **108**, 087601 (2012).
- 23. X. Li, T. Qiu, J. Zhang, E. Baldini, J. Lu, A.M. Rappe, K.A. Nelson. "Terahertz field-induced ferroelectricity in quantum paraelectric SrTiO<sub>3</sub>," *Science* **364**, 1079-1082 (2019).
- 24. A. de la Torre, D. M. Kennes, M. Claassen, S. Gerber, J. W. McIver, M. A. Sentef. "Nonthermal pathways to ultrafast control in quantum materials," *Reviews of Modern Physics*

- **93**, 041002 (2021).
- 25. Y. Zhang, J. Dai, X. Zhong, D. Zhang, G. Zhong, J. Li. "Probing Ultrafast Dynamics of Ferroelectrics by Time-Resolved Pump-Probe Spectroscopy," *Advanced Science* **8**, 2102488 (2021).
- 26. S. Prosandeev, J. Grollier, D. Talbayev, B. Dkhil, L. Bellaiche. "Ultrafast neuromorphic dynamics using hidden phases in the prototype of relaxor ferroelectrics," *Physical Review Letters* **126**, 027602 (2021).
- 27. A. S. Disa, T. F. Nova, A. Cavalleri. "Engineering crystal structures with light," *Nature Physics* **17**, 1087-1092 (2021).
- 28. D. Ji, S. Cai, T. R. Paudel, H. Sun, C. Zhang, L. Han, Y. Wei, Y. Zang, M. Gu, Y. Zhang, W. Gao, H. Huyan, W. Guo, D. Wu, Z. Gu, E. Y. Tsymbal, P. Wang, Y. Nie, X. Pan. "Freestanding crystalline oxide perovskites down to the monolayer limit," *Nature* **570**, 87-90 (2019).
- 29. S. P. Weathersby, G. Brown, M. Centurion, T. F. Chase, R. Coffee, J. Corbett, J. P. Eichner, J. C. Frisch, A. R. Fry, M. Gühr, N. Hartmann, C. Hast, R. Hettel, R. K. Jobe, E. N. Jongewaard, J. R. Lewandowski, R. K. Li, A. M. Lindenberg, I. Makasyuk, J. E. May, D. McCormick, M. N. Nguyen, A. H. Reid, X. Shen, K. Sokolowski-Tinten, T. Vecchione, S. L. Vetter, J. Wu, J. Yang, H. A. Dürr, X. J. Wang. "Mega-electron-volt ultrafast electron diffraction at SLAC National Accelerator Laboratory," *Review of Scientific Instruments* 86, 073702 (2015).
- 30. K. Y. Chan, W. S. Tsang, C. L. Mak, K. H. Wong, P. M. Hui. "Effects of composition of PbTiO<sub>3</sub> on optical properties of (1-x)PbMg<sub>1/3</sub>Nb<sub>2/3</sub>O<sub>3</sub>-xPbTiO<sub>3</sub> thin films," *Physical Review B* **69**, 144111 (2004).
- 31. F. Chen, Y. Zhu, S. Liu, Y. Qi, H. Y. Hwang, N. C. Brandt, J. Lu, F. Quirin, H. Enquist, P. Zalden, T. Hu, J. Goodfellow, M. J. Sher, M. C. Hoffmann, D. Zhu, H. Lemke, J. Glownia, M. Chollet, A. R. Damodaran, J. Park, Z. Cai, I. W. Jung, M. J. Highland, D. A. Walko, J. W. Freeland, P. G. Evans, A. Vailionis, J. Larsson, K. A. Nelson, A. M. Rappe, K. Sokolowski-Tinten, L. W. Martin, H. Wen, A. M. Lindenberg. "Reply to `Comment on `Ultrafast terahertz-field-driven ionic response in ferroelectric BaTiO<sub>3</sub>," *Physical Review B* **97**, 226102 (2018).
- 32. A. M. Lindenberg, S. L. Johnson, D. A. Reis. "Visualization of atomic-scale motions in materials via femtosecond X-ray scattering techniques," *Annual Review of Materials Research* 47, 425-449 (2017).
- 33. R. Blinc, J. Dolinšek, A. Gregorovič, B. Zalar, C. Filipič, Z. Kutnjak, A. Levstik, R. Pirc. "Local Polarization Distribution and Edwards-Anderson Order Parameter of Relaxor Ferroelectrics," *Physical Review Letters* **83**, 424-427 (1999).
- 34. E. M. Mannebach, R. Li, K.-A. Duerloo, C. Nyby, P. Zalden, T. Vecchione, F. Ernst, A. H. Reid, T. Chase, X. Shen, S. Weathersby, C. Hast, R. Hettel, R. Coffee, N. Hartmann, A. R. Fry, Y. Yu, L. Cao, T. F. Heinz, E. J. Reed, H. A. Dürr, X. Wang, A. M. Lindenberg. "Dynamic Structural Response and Deformations of Monolayer MoS<sub>2</sub> Visualized by Femtosecond Electron Diffraction," *Nano Letters* **15**, 6889-6895 (2015).
- 35. H. Liu, Z. Sun, S. Sun, Y. Zhang, H. Luo, H. Qi, L. Liu, J. C. Neuefeind, X. Xing, J. Chen. "Evolving Differentiated Local Polar Displacement and Relaxor Behavior in Pb(Mg<sub>1/3</sub>Nb<sub>2/3</sub>)O<sub>3</sub>–PbTiO<sub>3</sub> Perovskites," *Chemistry of Materials* **34**, 3985-3992 (2022).
- 36. S. B. Lang, W. M. Zhu, Z. G. Ye. "Specific heat of ferroelectric Pb(Zr1-xTix)O<sub>3</sub> ceramics across the morphotropic phase boundary," *Journal of Applied Physics* **111**, 094102 (2012).
- 37. V. A. Stoica, N. Laanait, C. Dai, Z. Hong, Y. Yuan, Z. Zhang, S. Lei, M. R. McCarter, A. Yadav, A. R. Damodaran, S. Das, G. A. Stone, J. Karapetrova, D. A. Walko, X. Zhang, L. W. Martin, R. Ramesh, L. Q. Chen, H. Wen, V. Gopalan, J. W. Freeland. *Nature Materials* 18, 377-383 (2019).

- 38. Y. Ahn, A. S. Everhardt, H. J. Lee, J. Park, A. Pateras, S. Damerio, T. Zhou, A. D. DiChiara, H. Wen, B. Noheda, P. G. Evans. *Physical Review Letters* **127**, 097402 (2021).
- 39. H. Wen, P. Chen, M. P. Cosgriff, D. A. Walko, J. H. Lee, C. Adamo, R. D. Schaller, J. F. Ihlefeld, E. M. Dufresne, D. G. Schlom, P. G. Evans, J. W. Freeland, Y. Li. *Physical Review Letters* **110**, 037601 (2013).
- 40. A. Kumar, J. N. Baker, P. C. Bowes, M. J. Cabral, S. Zhang, E. C. Dickey, D. L. Irving, J. M. LeBeau. "Atomic-resolution electron microscopy of nanoscale local structure in lead-based relaxor ferroelectrics," *Nature Materials* **20**, 62-67 (2021).
- 41. S. Lindemann, J. Irwin, G.-Y. Kim, B. Wang, K. Eom, J. Wang, J. Hu, L.-Q. Chen, S.-Y. Choi, C.-B. Eom, M.S. Rzchowski. "Low-voltage magnetoelectric coupling in membrane heterostructures," *Science Advances* 7, eabh2294.
- 42. A. Sood, X. Shen, Y. Shi, S. Kumar, J. Park Su, M. Zajac, Y. Sun, L.-Q. Chen, S. Ramanathan, X. Wang, W.C. Chueh, A.M. Lindenberg. "Universal phase dynamics in VO2 switches revealed by ultrafast operando diffraction," *Science* 373, 352-355 (2021).

# **TOC Graphic**

